Renewable and Sustainable Energy Reviews 207 (2025) 114997

Contents lists available at ScienceDirect

Renewable and Sustainable Energy Reviews

journal homepage: www.elsevier.com/locate/rser

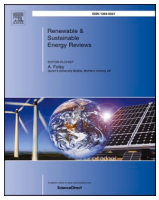

Solar tower power generation under future attenuation and climate scenarios

Jesús Polo [a,*], Shukla Poddar [b], Noelia Simal [c,d], Jesús Ballestrín [c,d], Aitor Marzo [d,e], Merlinde Kay [b], Elena Carra [c,d]

[a] Photovoltaic Solar Energy Unit (Energy Department CIEMAT), Avda. Complutense 40, 28040, Madrid, Spain
[b] School of Photovoltaic and Renewable Energy Engineering, University of New South Wales, Sydney, Australia
[c] CIEMAT-Plataforma Solar de Almería. Solar Concentrating Systems Unit, Almería, Spain
[d] CIESOL, Solar Energy Research Center, Joint Institute University of Almería - CIEMAT, Almería, Spain
[e] Department of Optics, University of Granada, Granada, Spain

ARTICLE INFO

Keywords:
Atmospheric attenuation
Solar tower plant performance
CMIP6 models
Climate change impact in solar power

ABSTRACT

This work presents a novel analysis of the potential impact of atmospheric attenuation in the performance of solar tower plants for future climate change scenarios (2030–2060). Atmospheric attenuation has been estimated from aerosol optical depth information in CMIP6 climatic models for several scenarios (optimistic and pessimistic in terms of mitigation actions taken). Atmospheric attenuation data derived from CMIP6 models was evaluated using the extensive and reliable experimental database at PSA (Plataforma Solar de Almería). Detailed modeling of a solar tower plant is also performed for the conditions at PSA showing a decrease in annual power production less than 2 % for 2030–2060 period. A global impact of atmospheric attenuation is analyzed in relative terms and global maps of future attenuation shows the specific regions more adversely affected in the optimistic and pessimistic future scenarios. According to impact of atmospheric attenuation in solar field efficiency, these results may help in the future planning of deployment for solar tower plants.

1. Introduction

At the COP28 climate change conference, over one hundred countries agreed to work towards tripling the capacity of renewable generation by 2030. This is in line with the net zero emissions 2050 scenario of the International Energy Agency (IEA). Solar energy is uniquely positioned to support the global energy transition and climate change goals, as well as to foster job creation and economic growth in the context of the Green Deal [1] and COP28 [2] goals. Over ten million people were directly and indirectly employed in the renewable energy industry [3]. In addition, the solar sector is today preparing the new ecosystem for green fuels and hydrogen production, solving one of the main drawbacks of energy storage and transportation [4]. Within the industrial sector of solar energy technologies, we can distinguish two main families: thermal concentrated solar power (CSP) and photovoltaic (PV). Although CSP is more efficient in terms of energy savings and has reliable and more efficient energy storage systems, PV energy production is currently more attractive, in financing terms, than CSP. This fact leads energy investors to lean more towards PV. However, the energy sector is highly competitive. In the search for new, more efficient and cost-effective solutions, new plant concepts are emerging. One example is hybrid CSP and PV plants, which take advantage of the best of both technologies.

Nevertheless, within the different technologies for solar energy systems, CSP with thermal storage ensures high dispatchability of the energy generated offering several advantages over other renewable energy systems. In addition, efficiency optimization of CSP is crucial in order to increase its competitiveness. Higher concentration ratio, enhanced receiver designs, thermal energy storage, better tracking systems and hybridization with other renewables are key aspects to the feasibility of CSP. In particular, solar tower plants with thermal storage based on molten salts allow to increase the efficiency because of the higher working temperature. Consequently, recent solar tower projects commissioned in 2018 and 2019 in China, Morocco and South Africa are large plants (over 100 MWe) with large thermal storage systems [5].

Solar tower plants are one of the CSP technologies, also known as central receiver technology. They have a very large solar field consisting of thousands of heliostats which track the Sun position and reflect the incident radiation to the receiver placed at the upper part of the tower.

* Corresponding author.
E-mail address: jesus.polo@ciemat.es (J. Polo).

https://doi.org/10.1016/j.rser.2024.114997
Received 20 March 2024; Received in revised form 10 May 2024; Accepted 10 October 2024
Available online 13 October 2024

Abbreviations:

ACCESS: Australian Community Climate and Earth System Simulator
BOM: Bureau of Meteorology
CMCC: Euro-Mediterranean Center on Climate Change
CMIP: Coupled Model Intercomparison Project
CSIRO: Commonwealth Scientific and Industrial Research Organization
CSP: Concentrated Solar Power
EC-Earth: Earth system model for the Coupled Model
GCM: Global Climate Models
IEA: International Energy Agency
MIROC: Model for Interdisciplinary Research on Climate
MPI: Max Planck Institute
MRI: Meteorological Research Institute
PSA: Plataforma Solar de Almería
PV: Photovoltaic
RCP: Representative Concentration Pathways
SAM: System Advisor Model
SSP: Shared Socio-economic Pathways
TMY: Typical Meteorological Year
TSEY: Typical Solar Extinction Year
WCRP: World Climate Research Programme

Notation/Symbols

β Extinction Coefficient (km^{-1})
AOD Aerosol Optical Depth
AT Attenuation
f Correction factor
p Significance level, p-value
S Slant range (km)

Units

m meter
MW MegaWatt
GWh GigaWatt hour
MWe Megawatt electric
W Watts
km kilometer

Table 1
Characteristics of CMIP6 models.

No	Model Name	Centre/Country	Resolution (°Lat × °Lon)
1	ACCESS-CM2	CSIRO-BOM, Australia	1.25 × 1.875
2	CMCC-CM2-SR5	CMCC, Italy	0.942 × 1.25
3	CMCC-ESM2	CMCC, Italy	0.942 × 1.25
4	EC-Earth3	EC-Earth-Consortium, Europe	0.72 × 0.72
5	MIROC-ES2L	MIROC, Japan	2.8 × 2.8
6	MIROC6	MIROC, Japan	1.4 × 1.4
7	MPI-ESM1-2-HR	MPI-M, Germany	0.935 × 0.938
8	MPI-ESM1-2-LR	MPI-M, Germany	1.865 × 1.875
9	MRI-ESM2-0	MRI, Japan	1.121 × 1.125

Energy efficiency in solar tower plants is influenced by the atmospheric attenuation taking place in the optical path between the heliostat and the receiver. The heliostat-receiver optical path may be as large as 1 km, or even larger in high power capacity plants. Among all the optical losses affecting to the image of the solar flux on the receiver, atmospheric attenuation due to the scattering of the reflected irradiance with the aerosol particles in the atmospheric boundary layer might be the process that contributes the most to the energy loss of the plant. Extensive studies on modeling and characterizing the atmospheric attenuation induced losses have been reported in the literature [6–15]. However, the number of works on measuring this phenomenon is still scarce [16–20], limiting thus the broadening of model validation [21,22].

Due to their dependency on the meterological parameters, any changes in the current climate can change their energy generation capacity. Several studies have projected changes in the future atmospheric conditions due to climate change, that might affect the system performance in the future years [23]. The impact of future climate projections on renewable energy systems performance has been recently analyzed in several works [23–25]. Analysis of long-term climate projections in Australia indicated a decline in Photovoltaic (PV) performance due to reduced insolation and increased temperatures [26,27]. On the other hand, impact of climate change on potential for distributed PV in Brazil studied in Brazil concluded the robustness of PV systems [28]. Nevertheless, detailed analysis of the impact of future climate scenarios on CSP, and particularly on large solar tower plants is still pending. A substantial increase in the aerosol load in the atmosphere, would negatively affect the optical performance of solar systems. In particular, the increase of aerosols contribute to decrease the optical efficiency of the solar field of heliostat in solar towers due mainly to the increase of the atmospheric attenuation. Some recent works confirmed the increase in the intensity of airborne particles in the Mediterranean countries due to African dust transportation towards western Mediterranean basin [29].

For exploring future climate conditions under different scenarios the Couple Model Intercomparison Project (CMIP) can provide state-of-the-art simulations using multiple global climate models (GCM). These models employ different greenhouse gas emission scenarios to simulate past, present, and future climate conditions. The sixth phase (CMIP6) is the latest generation of future climate projections with improvements in physical parameterizations [30].

The main novelty of this work consists of the first analysis, to our knowledge, of future changes in the atmospheric attenuation associated with different climate change scenarios, and their impact on solar tower plant performance. For this purpose, data of aerosol optical depth (AOD) from CMIP6 models are used as input to compute atmospheric attenuation worldwide on a monthly basis for different future scenarios for the period 2030–2060. In addition, detailed analysis is performed for a reference plant using the meteorological and solar radiation input for a site in south-east Spain, where long term measurements of attenuation have been monitored since 2017. The confidence in the worldwide quantitative results of this study is challenging due to the scarcity of experimental reliable information on atmospheric attenuation worldwide, and thus we have used the most reliable experimental database on atmospheric attenuation to assess the modeling results in one specific site. The relative analysis performed offers relevant information on expected changes in atmospheric attenuation and consequently in the optical efficiency of the solar field that is of high interest for the solar tower plant locations and future performance.

2. Climate model projections from future scenarios in CMIPI6 models for atmospheric attenuation

This study uses CMIP6 model data (https://esgf-node.llnl.gov/search/cmip6/) to analyze the impact of climate change on solar tower plants [31]. The World Climate Research Programme's (WCRP) CMIP6 simulations are the most recent global model climate projections representing the earth's past and the future climate under different scenarios. The recent generation CMIP6 models have higher resolutions, improved

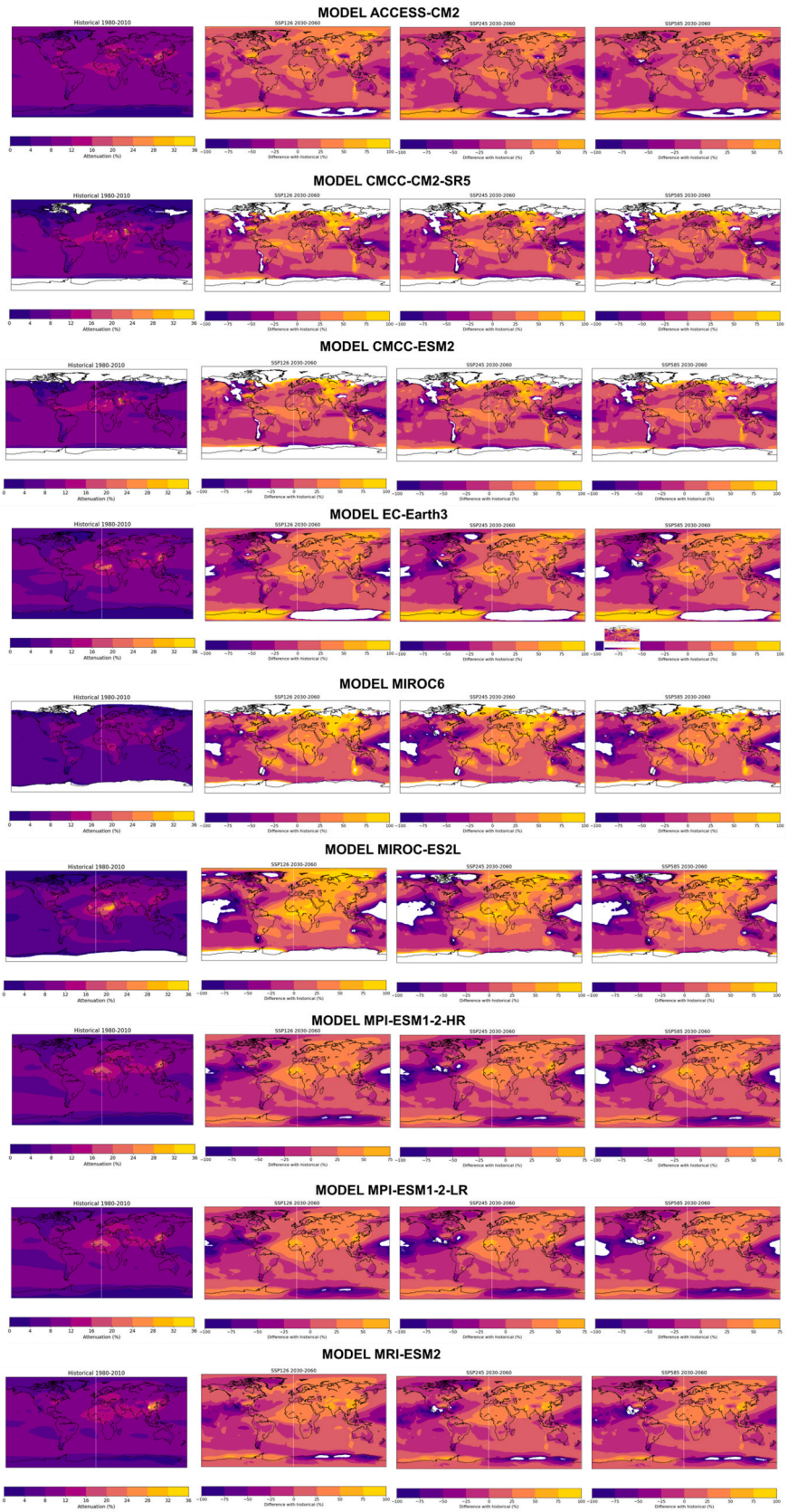

Fig. 1. Atmospheric attenuation maps for the nine CMIP6 models used in this study. The columns show the mean atmospheric attenuation for the historical and future period under SSP126, SSP245 and SSP585 scenarios, respectiveley.

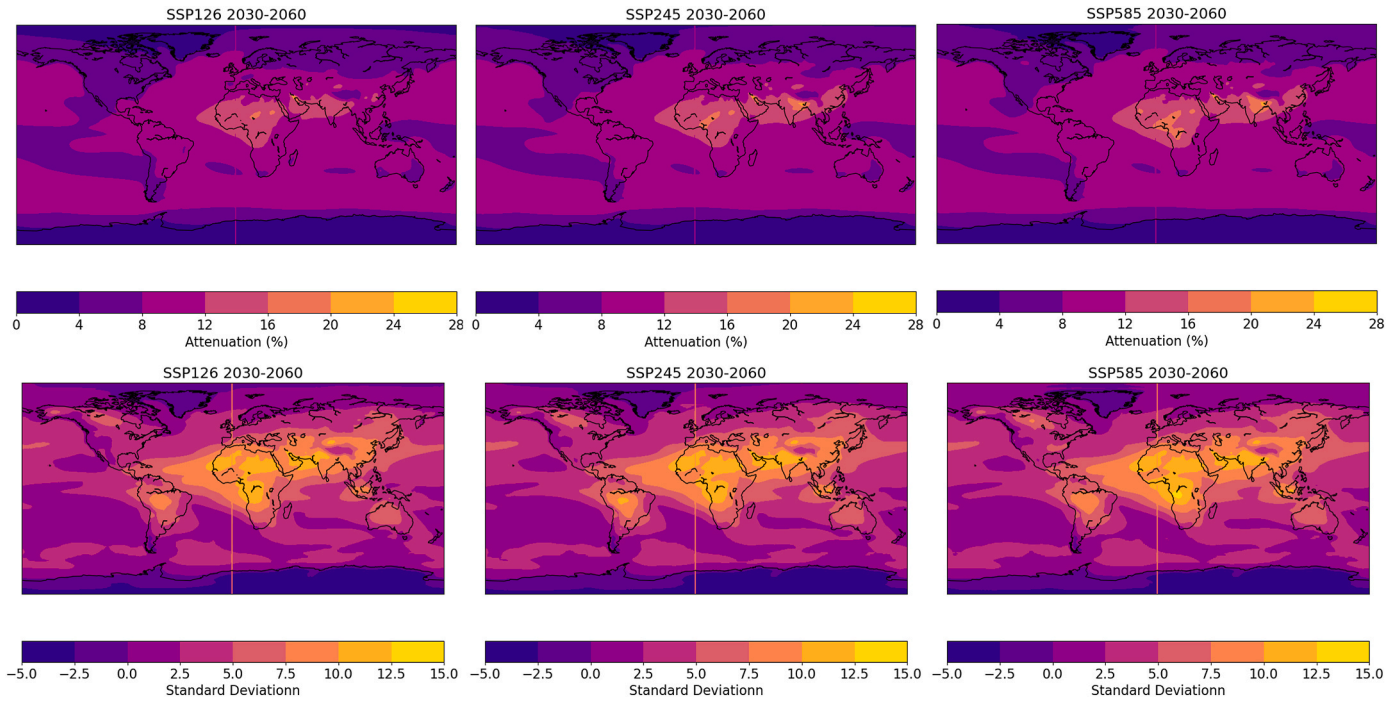

Fig. 2. Mean attenuation and standard deviation maps for future scenarios from all models together.

representation of physics and more information incorporated in the scenario-design, along with several improvements in the aerosol representation in the models. Several models under CMIP6 have interactive aerosols schemes to include a more sophisticated description of aerosols direct and/or indirect effects. The future climate is simulated for a wide-range of future scenarios and are available in a standardized format as part of the Scenario Model Intercomparison Project (ScenarioMIP) [32,33]. Each scenario in ScenarioMIP is designed to study the climate response to different natural and anthropogenic forcings based on different shared socio-economic pathways (SSP) and representative concentration pathways (RCP).

In this study we focus on historical projections along with three future climate scenarios – SSP126 (green growth path), SSP245 (midway path) and SSP585 (fossil fueled development). These scenarios are described below [34].

- SSP126 scenario: an optimistic scenario with low challenges to both mitigation and adaptation. An additional radiative forcing of 2.6 W m^{-2} by the year 2100 is assumed here, considering that climate protection measures will be taken.
- SSP245 scenario: intermediate scenario corresponding to medium challenges to mitigation and adaptation. This is a medium pathway of future greenhouse gas emissions with an additional radiative forcing of 4.5 W m^{-2}.
- SSP585 scenario: pessimistic scenario with high challenges to mitigation and low challenges to adaptation. Additional radiative forcing of 8.5 W m^{-2} is considered in this scenario.

We analyze two periods of interest – historical period (1980–2010) and future period (2030–2060). In this study, we use nine CMIP6 models that have time-varying future aerosols for all the scenarios and time periods of interest (Table 1). All the analysis has been performed using monthly aerosol optical depth (AOD) data. We have re-gridded all the models to a common resolution of 0.5° × 0.5° to compare them, using a bilinear interpolation technique.

Each gridded AOD dataset was used to compute the 50th percentile of AOD along each pixel in both historical and future scenarios for each CMIP6 model. This value was used as input to a model to compute atmospheric attenuation at 1 km of slant range that employs AOD as turbidity input. The model used was developed by Polo et al. from multiple radiative transfer calculations, and it was validated at PSA (Plataforma Solar de Almería), in south-east Spain [9,10].

Polo's model computes the atmospheric attenuation, in percentage, from the slant range and AOD by the following expression,

$$AT(\%) = f\left[a\,S^3 + b\,S^2 + c\,S + d\right] \tag{1}$$

Where S is the heliostat-receiver optical path expressed in km, and the polynomial coefficients a,b,c and d are determined from the AOD values by,

$$\begin{aligned} a &= 3.13\,AOD^3 - 1.96\,AOD^2 + 1.60\,AOD - 0.133 \\ b &= -14.74\,AOD^3 + 2.49\,AOD^2 - 11.85\,AOD + 0.544 \\ c &= 28.32\,AOD^3 - 7.57\,AOD^2 + 48.74\,AOD + 0.371 \\ d &= -2.61\,AOD^3 + 3.70\,AOD^2 - 2.64\,AOD + 0.179 \end{aligned} \tag{2}$$

Finally, the correction factor f is defined also as a function of the AOD by,

$$f = \begin{cases} 2.874\,e^{-3.059\,AOD} - 7.445e^{-114.7\,AOD} & AOD \le 0.05 \\ 2.358\,e^{-7.094\,AOD} + 0.836e^{-0.141\,AOD} & AOD > 0.05 \end{cases} \tag{3}$$

Physically speaking, atmospheric attenuation follows an exponential law with the extinction coefficient at the boundary layer (β) [35],

$$AT(\%) = 100\,\left(1 - e^{-\beta\,S}\right) \tag{4}$$

However, for practical and historical reasons, atmospheric attenuation data have been frequently fitted to a third order polynomial [6]. Consequently most of the models for estimating the solar flux distribution at the receiver such as DELSOL [36] and MIRVAL [37], for optimizing the heliostat field such as SolarPILOT [38] and SolTrace [39], and for plant performance analysis such as SAM (System Advisor Model) model the atmospheric attenuation using the coefficients of a third order polynomial as input [40]. Therefore, the modeling procedures advise to develop atmospheric attenuation models in a polynomial form to make easier the implementation in modeling tools, and that was the main reason to express the Polo's model in polynomial form.

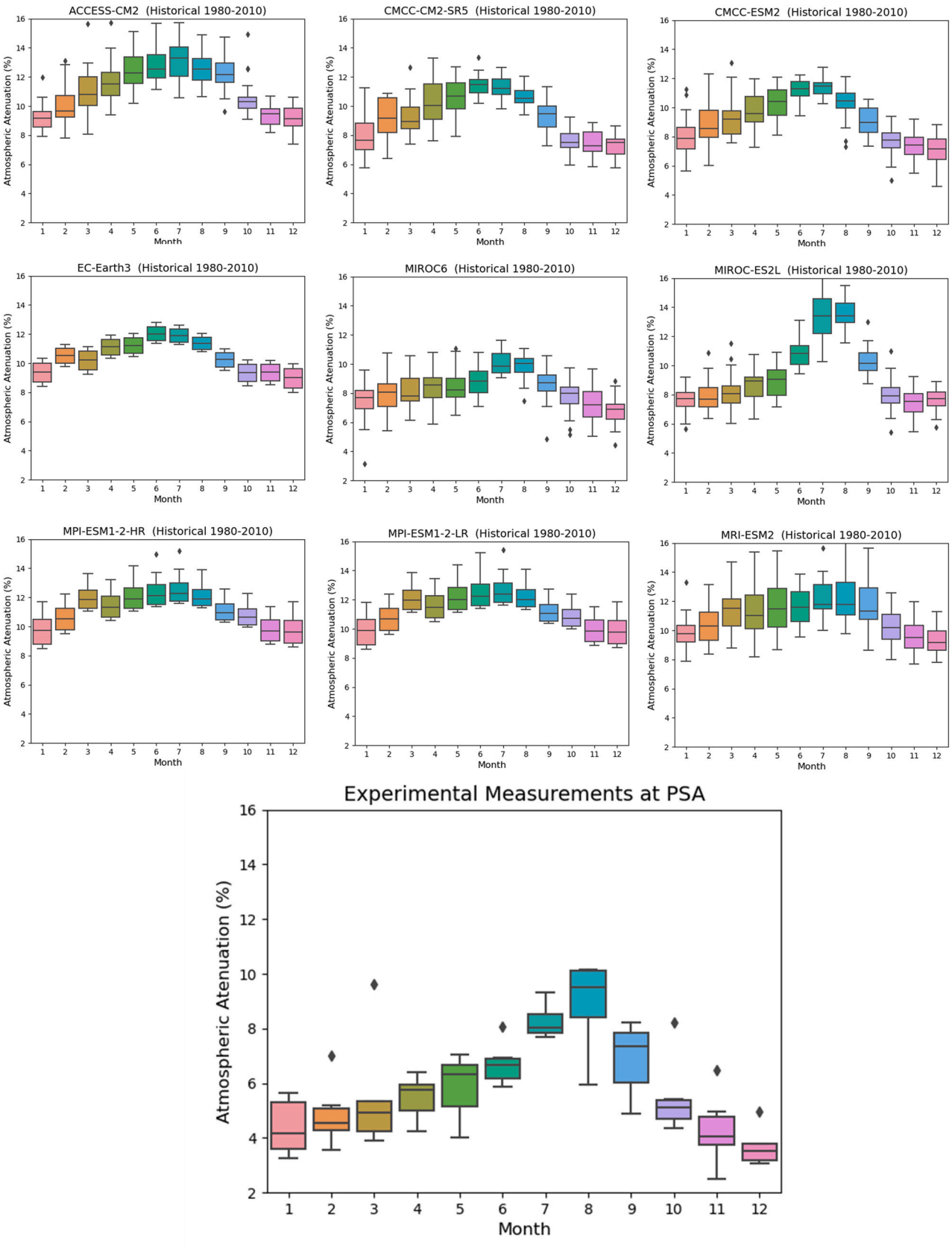

Fig. 3. Box-plot of monthly attenuation in models historical database and for the experimental values of atmospheric attenuation in PSA.

Table 2
50th percentile of the historical and future scenarios atmospheric attenuation in CMIP6 models at PSA site.

CMIP6 Model	Historical (%)	SSP126 (%)	SSP245 (%)	SSP585 (%)
ACCESS-CM2	11.2	9.4	9.9	9.9
CMCC-CM2-SR5	9.3	8.7	9.0	9.1
CMCC-ESM2	9.2	8.7	9.0	9.2
EC-Earth3	10.4	8.8	9.0	9.0
MIROC6	9.4	8.2	8.5	8.7
MIROC-ES2L	8.3	5.7	6.2	6.5
MPI-ESM1-2-HR	11.2	9.5	9.6	9.7
MPI-ESM1-2-LR	11.3	9.5	9.7	9.8
MRI-ESM2	11.1	9.6	9.9	9.9

Table 3
Polynomial coefficients corresponding to monthly attenuation mean values measured at PSA.

Month	Polynomial
Jan	$AT = 0.00002\,S^3 - 0.00148\,S^2 + 0.05493\,S + 0.00003$
Feb	$AT = 0.00004\,S^3 - 0.00229\,S^2 + 0.06883\,S + 0.00006$
Mar	$AT = 0.00004\,S^3 - 0.00229\,S^2 + 0.06883\,S + 0.00006$
Apr	$AT = 0.00006\,S^3 - 0.00327\,S^2 + 0.08266\,S + 0.00012$
May	$AT = 0.00006\,S^3 - 0.00327\,S^2 + 0.08266\,S + 0.00012$
Jun	$AT = 0.00010\,S^3 - 0.00448\,S^2 + 0.09738\,S + 0.00022$
Jul	$AT = 0.00014\,S^3 - 0.00574\,S^2 + 0.11100\,S + 0.00035$
Aug	$AT = 0.00025\,S^3 - 0.00884\,S^2 + 0.13971\,S + 0.00080$
Sep	$AT = 0.00010\,S^3 - 0.00448\,S^2 + 0.09738\,S + 0.00022$
Oct	$AT = 0.00004\,S^3 - 0.00229\,S^2 + 0.06883\,S + 0.00006$
Nov	$AT = 0.00002\,S^3 - 0.00148\,S^2 + 0.05493\,S + 0.00003$
Dec	$AT = 0.00002\,S^3 - 0.00148\,S^2 + 0.05493\,S + 0.00003$

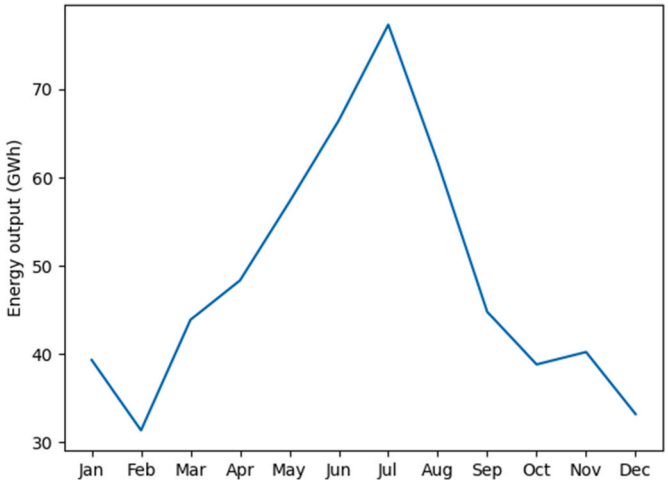

Fig. 4. Monthly generation of reference solar tower plant at PSA for the experimental measurements of atmospheric attenuation.

In this study, the statistical significance of the future change results is examined at each grid point using Student's t-test at 5 % significance level ($p < 0.05$). The results are denoted using the convention adapted from Tebaldi et al. to identify the regions with statistically significant change [41]. Following this convention, we represent the results as areas with significant agreement, insignificant agreement, and significant disagreement.

- Grid points showing substantial concurrence among the models are highlighted using color and stippling. These grid points represent locations where at least half of the models are significant, with at least 70 % of those members concurring on the direction of change. These regions have higher confidence in future change.
- The areas with insignificant agreement between the models are denoted in color. At these grid points, less than 50 % of the models are significant, leading to low confidence in future changes.
- The areas represented in white are the regions with significant disagreement between the models. At these grid points at least half of the ensemble members show a significant change, and <70 % of those members agree on the direction of change. These regions have limited confidence in future change due to significant model disparity.

3. Results

3.1. Global atmospheric attenuation

To assess the atmospheric attenuation worldwide, we estimated the mean and standard deviation of the attenuation for the historical (1980–2010) and future (2030–2060) period under various climate change scenarios. Fig. 1 shows the maps of the 50th percentile of the atmospheric attenuation for 1 km of heliostat-receiver optical path computed for each CMPI6 model using the attenuation model described above. High similarity in the spatial distribution of the atmospheric attenuation can be found in the historical results of all the models. Higher atmospheric attenuation is generally found in Sahara, Arabian Peninsula, India, China and south-east Asia. Very high values predicted by some models are observed. Thus, CMCC family models for the Persian Gulf area predict attenuation levels over 30 %. MIROC-ES2L predict also over 30 % of atmospheric attenuation in Sudan and Chad area. Finally, south China exhibits very high atmospheric attenuation in the MRI-ESM2 predictions. This is mainly due to the historical forcing, model behavior in the individual models.

The relative difference between the 50th percentile of 30 years (2030–2060) of future monthly attenuation for each scenario and the 50th percentile of the historical attenuation can be seen in Fig. 1. Significant increase in the atmospheric attenuation for some part of the world can be observed in all the models under different future scenarios. Among all the models, MIROC family predicts the highest increase of atmospheric attenuation, particularly in Africa and Asia continents.

Fig. 2 shows the maps of the mean of the 50th percentile attenuation of all models for the future scenarios and the standard deviation. Highest attenuation values are distributed along Africa, Arabian Peninsula, India and China regions, with slightly increasing values predicted from the optimistic scenario to the most pessimistic one. On analyzing the future changes in mean attenuation, we observe significant increases in most parts of the world under all the scenarios. Even though the spatial pattern for the changes in attenuation remain consistent in the future, we can see a significant increase in the values under SSP585 than the other two lower emission scenarios. In addition, the standard deviation maps show also that the higher deviation from the mean is observed generally in the Sun Belt region.

3.2. Analysis of the results for PSA site

One of the main problems in dealing with atmospheric attenuation and its impact in solar tower plants is the scarcity and difficulties of finding reliable measurements. However, atmospheric attenuation values have been monitored, from June 2017 to July 2023, at Solar Platform of Almeria (PSA). PSA is the largest experimental facility for CSP systems, located in Tabernas (Almería) in the southeast Spain. The experimental system consists of two very high resolution cameras that take simultaneous continuous images of a Lambertian target of 2 × 2 m. The position and calibration of the two cameras and the statistical post-processing of the pixels allow the determination of the atmospheric attenuation at 742 m with an absolute error of ±2 %, which is the distance between the two cameras. The extinction coefficient is also determined from the imagery allowing thus to extrapolate the atmospheric attenuation to other optical paths. Specific details of this

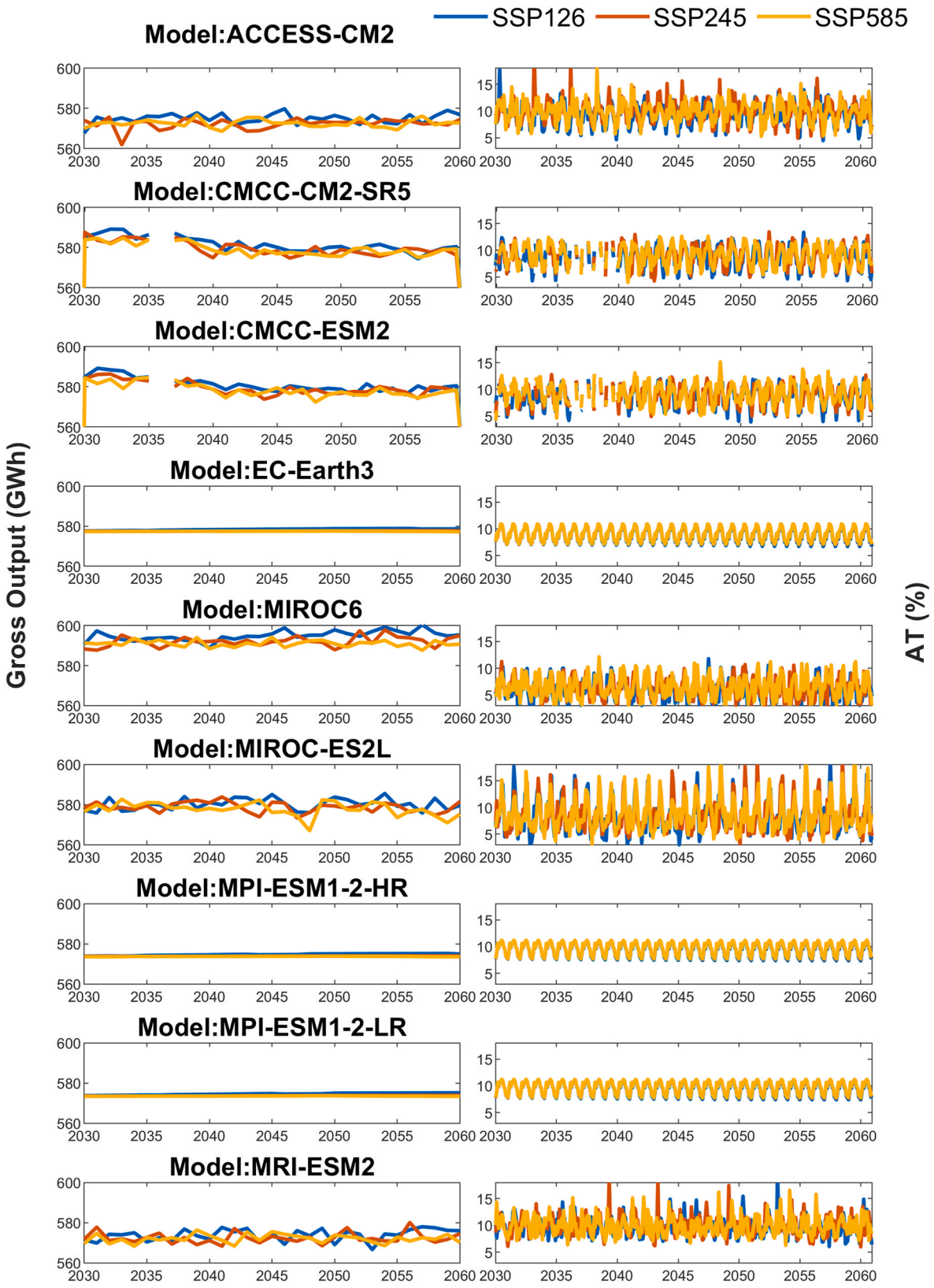

Fig. 5. Annual gross energy estimation of a reference solar tower plant for 2030–2060 in CMIP6 models and monthly attenuation.

experimental system and description of the database can be found in previous works [17,18,22,42]. Therefore, PSA likely offers the longest and highest accurate experimental database on atmospheric attenuation. Detailed statistical analysis of the whole experimental data at PSA has been recently performed making possible the construction of a statistical representative year of extinction named as Typical Solar Extinction Year (TSEY) [43].

Fig. 3 shows the model mean monthly box and whisker plots for the

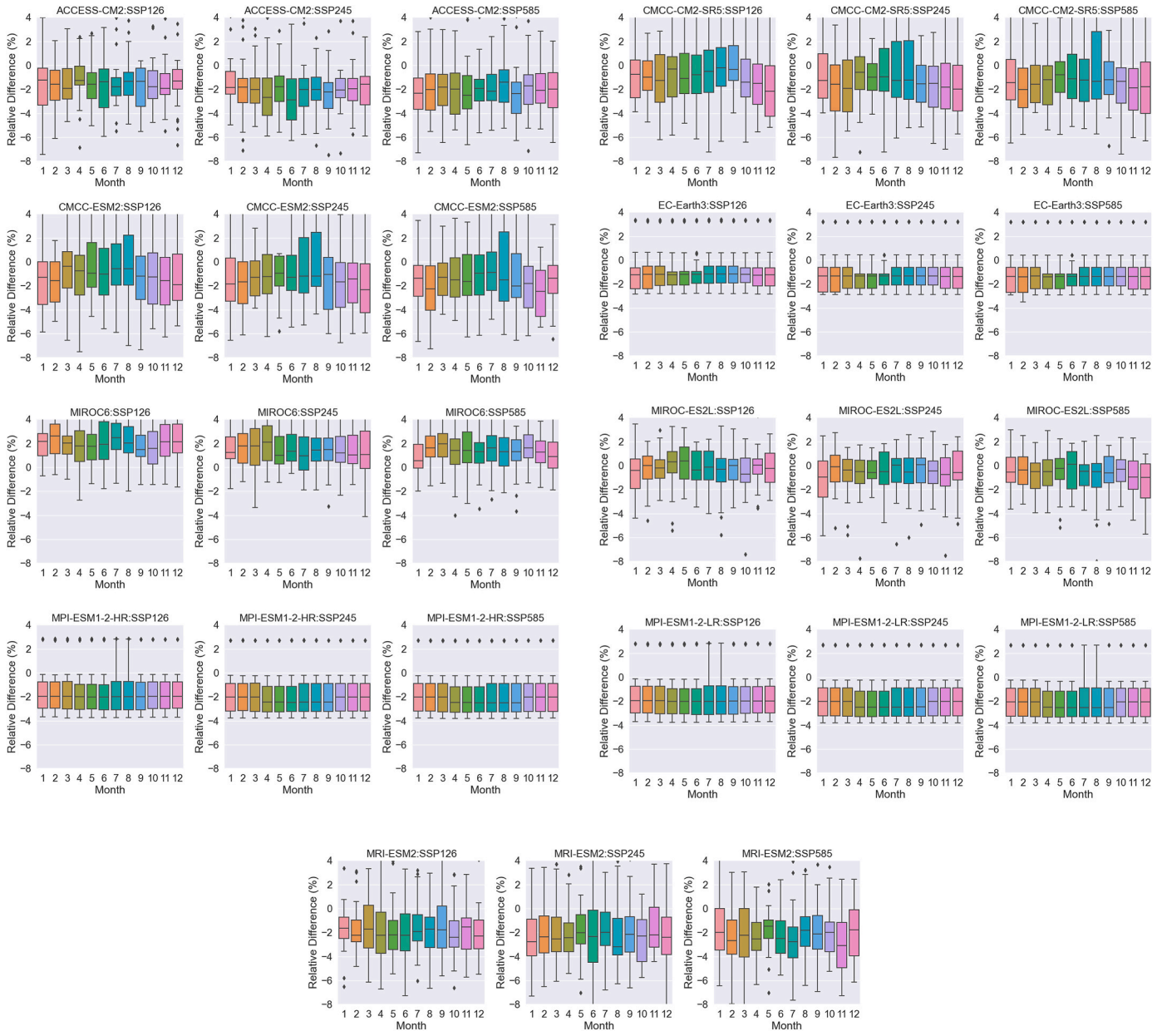

Fig. 6. Box and Whisker plots for the relative difference in gross energy generated by a solar tower plant for future scenarios (2030–2060) when compared with the generation estimated for the PSA using the experimental attenuation values.

historical period along with individual models used in this study for PSA location. A seasonal pattern can be easily visible in the plots, with higher values during summer.

In addition, the monthly measurements of the atmospheric attenuation at PSA at 742 m is also shown as box and whisker plot in the bottom of the figure to illustrate the complete experimental database available. Atmospheric attenuation measurements at 742 m vary between 3 and 5% in winter to 8–10 % during summer. The models show a similar seasonal trend like the observations which gives us confidence in the results related to future climate scenarios. Quantitative comparison should be taken with care since the experimental attenuation values correspond to an optical path of 742 m and the estimated attenuation values are for 1 km of heliostat-receiver distance. The expected attenuation values at PSA for 1 km of optical path can be roughly estimated by adding around 2 % of attenuation to the measuring values at 742 m in the AOD prevailing conditions of the site.

Table 2 presents the 50th percentile of the monthly atmospheric attenuation computed from the historical data and for future scenarios of the CMIP6 models for the PSA site. All the CMPI6 models predicted similar attenuation values for future scenarios, excepting MIROC-ES2L which estimate lower attenuation for all the scenarios. These values are consistent with previous studies showing a reduction of aerosols in most part of Europe for CMIP6 climate projections [44]. In all the models SSP585 scenario (the most pessimistic one) resulted in slightly higher attenuation than SSP126 (the most optimistic one). The mean monthly attenuation value from PSA measurements was 5.8 % at 742 m, and could be estimated approximately to around 8 % at 1 km, which is closer to the predictions of most CMIP6 models. Besides, the intra-annual profile of the monthly atmospheric attenuation in MIROC-ES2L resulted in great agreement with the experimental measurements at PSA.

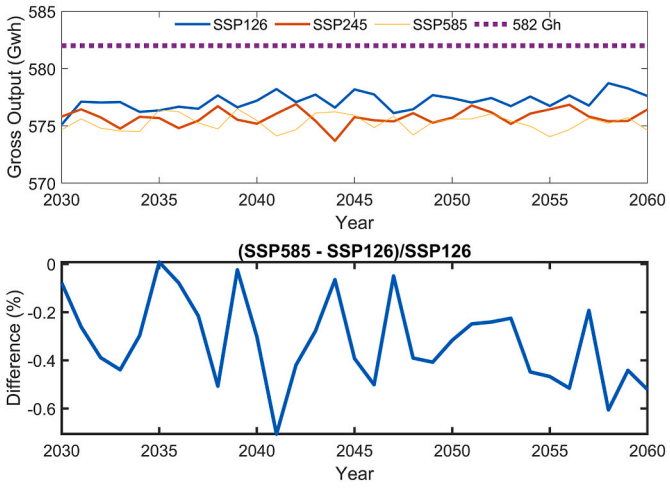

Fig. 7. Generation of a solar tower plant at PSA with the ensemble of all CMIP6 models.

3.3. Impact on a solar tower reference plant

Modeling of a reference plant based on Crescent Dunes has been performed to analyze the potential impact of future scenarios on plant energy production using the PSA site information. Crescent Dunes plant, placed in the state of Nevada (EEUU), is a molten salt solar tower of 110 MW with a solar field of 10000 heliostats surrounding a 195 m height tower. The thermal storage capacity is of 10 h. For the meteorological input to model the plant performance a typical meteorological year (TMY) obtained from Meteonorm for PSA coordinates was used. The plant modeling was perform with PySAM library. PySAM is a python package which makes calls to SAM (System Advisor Model) simulation Core [45]. PySAM is very versatile and a much better tool to be used for the scope of this work than SAM user interface, since the input parameters of the plant can be changed dynamically in a loop.

The first step in modelling the reference plant generation consisted of using the TMY as meteorological input and the different attenuation polynomial coefficients for each month corresponding to the mean attenuation values measured at PSA. This procedure can be done straightforwardly in PySAM by input dynamically the corresponding coefficients month by month in a loop. Table 3 lists the twelve different polynomials used in modelling the reference plant at PSA. The total gross annual generation for TMY at PSA resulted from SAM modeling was 582 GWh. The monthly generation is shown in Fig. 4. The results of the annual and monthly gross energy of the plant for the attenuation experimental measurements can be considered as a snapshot of the current potential generation of a solar tower plant like Crescent Dunes at PSA site. Moreover, these estimations can be used to perform relative comparisons with the results of modeling future scenarios with CMIP6 models.

Therefore, the next step for analyzing the impact of future scenarios of atmospheric attenuation in solar tower power generation consisted in modeling the reference plant with the different monthly polynomials corresponding to the monthly attenuation values derived from the 2030–2060 predictions by CMIP6 models for each scenario. Consequently, for each model and scenario 30 years of hourly generation were modeled using in every month the corresponding attenuation predicted by the model. Monthly attenuation values and the corresponding coefficients of the third order polynomial were estimated with the Polo et al. model described in section 2. Fig. 5 shows the annual gross energy predicted for every scenario and model for the period 2030–2060 along with the corresponding monthly attenuation. In all models SSP126 scenario resulted generally to higher energy generation. Considering the estimated generation of 582 GWh as a reference of the today's potential generation of a reference solar tower plant at PSA site, all the models excepting CMCC family and MIROC6 estimated lower generation than the reference. The SSP585 scenario predict lower energy than the optimistic SSP126. This is due to higher atmospherics aerosols represented in SSP585, which affects the net generation capacity. Models E-Earth3 and MPI family produces constant predictions of the annual power generated since they model the aerosol load in a rather steady-state pattern with very low variation year by year.

Fig. 6 shows the box and whisker plots of the relative difference between the monthly gross energy predicted for every model and scenario and the monthly gross energy estimated as a reference of the current climatic situation at PSA (i.e. the corresponding values of Fig. 4). The predicted generation in future scenarios resulted in a maximum reduction of 4–5% of monthly energy generation. It can be remarked the general increase of energy predicted by MIROC6 model, as opposed to the other model predictions. On the other hand, there was no seasonal particular pattern in the relative differences in any model. In CMCC family and in ACCESS model the pessimistic scenarios had larger deviations in the monthly predictions than the optimistic (the interquartile distance is larger). In EC-Earth3 model and MPI family the predictions were very steady through the years.

Fig. 7 shows the annual generation of the reference solar tower plant at the PSA site for future scenarios using the mean monthly attenuation values for all the models tested in this work along with the current generation modeled with the experimental data (582 GWh). In addition Fig. 7 also shows the relative difference in annual generation between the optimistic (SSP126) and the most pessimistic (SSP585) scenarios. The gross energy generation with the ensemble of CMIP6 models presented a nearly steady evolution along the 30 years with a global reduction in about 5–7 GWh depending on the scenario. SSP126 scenario showed a lower energy reduction in all the future period (compared to the other two more pessimistic scenarios). However, the difference between the most pessimistic and the most optimistic scenario exhibited a slight increasing reduction trend along the years indicating the negative impact of the most pessimistic predictions in the long term.

3.4. Worldwide estimated impact

Fig. 8 shows the relative increase of the monthly mean of atmospheric attenuation worldwide according to the ensemble of all models for two scenarios (the most optimistic SSP126 and the most pessimistic SSP585). The difference is estimated with respect the historical estimation of all the models. The independent samples *t*-test was used to evaluate the statistical significance of the differences between historical and future attenuation, rejecting the null hypothesis for p-value <0.05. In addition, the maps shows the sites of solar tower plants of at least 50 MW of capacity (https://solarpaces.nrel.gov/by-technology/power-tower). Highest increase of atmospheric attenuation was in the range of 20 % for the optimistic scenario (SSP126) and over 40 % in the case of the pessimistic (SSP585). The greatest increase of attenuation was concentrated in Africa and India areas. According to these models and their predictions, the current locations of solar tower plants do not show such significant increment of the expected atmospheric attenuation in the future years.

4. Conclusions

CSP based on central receiver technology with molten salt thermal storage is very promising in energy dispatchability with higher efficiency in the thermal thermodynamic cycles compared to other solar technologies. The solar field efficiency in these type of plants has many challenges, with several optical aspects that depend on the components quality, operational management and meteorological conditions. Among all of them, the attenuation processes of the reflected solar radiation from the heliostats affected by the turbidity load in the optical path towards the receiver can have a significant negative impact in the

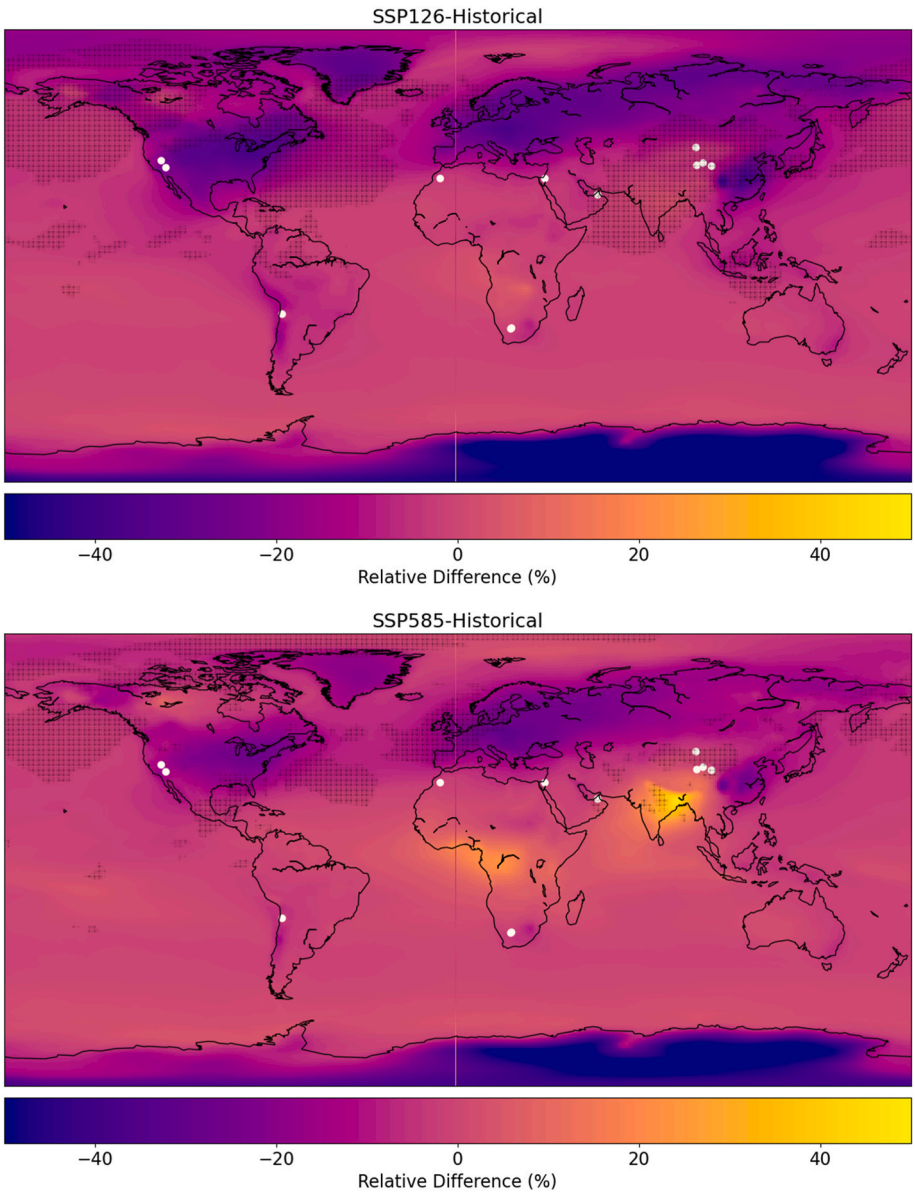

Fig. 8. Estimated impact of atmospheric attenuation for optimistic and pessimistic scenarios (2030–2060) of CMIP6 models. The white dots represent the location of current solar tower plants of at least 50 MW of capacity. Black dashed areas denote statistical significance according to *t*-test (p-value <0.05).

plant performance. The atmospheric attenuation effect depends on the airborne particle density in the atmospheric boundary layer (the lowest layer of atmosphere close to ground). Therefore the different current and future climatic conditions act as a highly conditioning actor for the solar towers deployment.

Climate change predictions for the future years may result in very adverse conditions for this kind of technology, depending on the mitigation actions to prevent the increase of atmospheric aerosols associated with emissions from human activity. Modeling aerosols for future scenarios in climate models offers a good input data for studying future scenarios for solar tower plants.

In this work, AOD data on a monthly basis from nine CMIP6 models is used as input information to analyze the impact of different future scenarios for 2030–2060 in the atmospheric attenuation worldwide. Atmospheric attenuation is computed from AOD data for nine CMIP6 models with three scenarios covering both optimistic and pessimistic assumptions in terms of mitigation actions of climate change. The confidence of the results are limited by the scarcity of the experimental information on atmospheric attenuation. Reliable experimental database on attenuation was acquired at PSA (Almeria, Spain) since 2017, by a very high-resolution system of cameras. Therefore, the large and accurate experimental database at PSA is used here to evaluate statistically the atmospheric attenuation estimated from the CMIP6 models, and detail modeling of a reference solar tower plant based on Crescent Dunes plant was done for the PSA conditions using the future projections of CMIP6 models.

The results of this study indicate that Africa and India regions showed an increase of the atmospheric attenuation up to 40 % for the pessimistic scenario and around 20 % for the optimistic case for the period 2030–2060. On the contrary, Europe and North America showed a reduction in the predicted future attenuation in all the scenarios. Therefore, not significant changes are observed in the models predictions for the current locations of most solar tower plants. The annual gross energy output for a reference solar tower plant, at PSA site, applying the CMIP6 attenuation data for PSA site could drop less than 2 % due to atmospheric attenuation processes.

CRediT authorship contribution statement

Jesús Polo: Conceptualization, Methodology, Investigation, Formal analysis, Writing – original draft. **Shukla Poddar:** Formal analysis, Methodology, Investigation, Resources, Writing – review & editing. **Noelia Simal:** Software, Validation, Resources. **Jesús Ballestrín:** Formal analysis, Resources, Writing – review & editing. **Aitor Marzo:** Formal analysis, Resources, Writing – review & editing. **Merlinde Kay:** Formal analysis, Resources, Writing – review & editing. **Elena Carra:** Software, Validation, Resources.

Declaration of competing interest

The authors declare that they have no known competing financial interests or personal relationships that could have appeared to influence the work reported in this paper.

Acknowledgements

The authors sincerely thank the HELIOSUN project (More efficient Heliostat Fields for Solar Tower Plants) with reference PID2021-126805OB-I00, funded by the Spanish MCIN/AEI/10.13039/5011000011033/FEDER, UE, and the MAPVSpain Project (PID2020-118239RJ-I00) financed by the Ministry of Science and Innovation and co-financed by the European Regional Development Fund (FEDER). The authors would like to thank World Climate Research Programme, for CMIP6 model outputs, the Earth System Grid Federation (ESGF) for archiving the data and providing access. The authors also thank the Australian National Computational Infrastructure (NCI) for providing computational resources for this work. The corresponding author wish to recognize the effort in several topics of solar resource knowledge by the experts group of IEA-PVPS Task 16, where atmospheric attenuation is included and fruitful discussion on the topic have been arisen. Authors also acknowledge ANID/FONDAP/1523A0006 “Solar Energy Research Center”, SERC-Chile. A. Marzo wish to thank the Ramón y Cajal contract (RYC2021-031958-I), funded by the Spanish Ministerio de Ciencia e Innovación MCIN/AEI/10.13039/501100011033 and by the European Union “NextGenerationEU/PRTR.

Data availability

Data will be made available on request.

References

[1] E. Commission. The European Green Deal. COM 2019:640. 2019, https://eur-lex.europa.eu/resource.html?uri=cellar:b828d165-1c22-11ea-8c1f-01aa75ed71a1.0002.02/DOC_1&format=PDF.
[2] UNFCCC. COP28 agreement signals “beginning of the end” of the fossil fuel era | UNFCCC. https://unfccc.int/news/cop28-agreement-signals-beginning-of-the-end-of-the-fossil-fuel-era; 2023.
[3] Irena ILO. Renewable energy and jobs: Annual Review. 2023. ISBN: 978-92-9260-552-0.
[4] Kane MK, Gil S. Green Hydrogen: a key investment for the energy transition. World Bank Blogs; 2022. https://blogs.worldbank.org/ppps/green-hydrogen-key-investment-energy-transition.
[5] Merchán RP, Santos MJ, Medina A, Calvo Hernández A. High temperature central tower plants for concentrated solar power: 2021 overview. Renew Sustain Energy Rev 2022;155:111828. https://doi.org/10.1016/J.RSER.2021.111828.
[6] Vittitoe CN, Biggs F. Terrestrial propagation LOSS, presented amer. Sec. ISES meeting., sandia report SAND78-1137C. 1978.
[7] Tahboub Z, Oumbe A, Hassar Z, Obaidli A. Modeling of irradiance attenuation from a heliostat to the receiver of a solar central tower. Energy Proc 2014;49:2405–13. https://doi.org/10.1016/j.egypro.2014.03.255.
[8] Shen Y, Jia B, Wang C, Yang W, Chen H. Numerical simulation of atmospheric transmittance between heliostats and heat receiver in Tower-Type solar thermal power station. Sol Energy 2023;265:112107. https://doi.org/10.1016/J.SOLENER.2023.112107.
[9] Polo J, Ballestrín J, Carra E. Sensitivity study for modelling atmospheric attenuation of solar radiation with radiative transfer models and the impact in solar tower plant production. Sol Energy 2016;134:219–27. https://doi.org/10.1016/j.solener.2016.04.050.
[10] Polo J, Ballestrín J, Carra E. Assessment and improvement of modeling the atmospheric attenuation based on aerosol optical depth information with applicability to solar tower plants. Energy 2020;208:118399. https://doi.org/10.1016/j.energy.2020.118399.
[11] Polo J, Ballestrín J, Alonso-Montesinos J, López-Rodriguez G, Barbero J, Carra E, Fernández-Reche J, Bosch JL, Batlles FJ. Analysis of solar tower plant performance influenced by atmospheric attenuation at different temporal resolutions related to aerosol optical depth. Sol Energy 2017;157:803–10. https://doi.org/10.1016/j.solener.2017.09.003.
[12] Hanrieder NM. Determination of Atmospheric Extinction for Solar Tower Plants Bestimmung der atmosphärischen Extinktion in solaren Turmkraftwerken. Hochschule Aachen; 2016. Thesis in technischen.
[13] Hanrieder N, Wilbert S, Pitz-Paal R, Emde C, Gasteiger J, Mayer B, Polo J. Atmospheric extinction in solar tower plants: absorption and broadband correction for MOR measurements. Atmos Meas Tech 2015;8:3467–80. https://doi.org/10.5194/amt-8-3467-2015.
[14] Hanrieder N, Sengupta M, Xie Y, Wilbert S, Pitz-Paal R. Modeling beam attenuation in solar tower plants using common DNI measurements. Sol Energy 2016;129:244–55. https://doi.org/10.1016/j.solener.2016.01.051.
[15] Ballestrín J, Marzo A. Solar radiation attenuation in solar tower plants. Sol Energy 2012;86:388–92. https://doi.org/10.1016/j.solener.2011.10.010.
[16] Hanrieder N, Wehringer F, Wilbert S, Wolfertstetter F, Pitz-Paal R, Campos VQ, Quaschning V. Determination of beam attenuation in tower plants. In: SolarPACES; 2012. p. 2012.
[17] Ballestrín J, Carra E, Monterreal R, Enrique R, Polo J, Fernández-Reche J, Barbero J, Marzo A, Alonso-Montesinos J, López G, Batlles FJJ. One year of solar extinction measurements at Plataforma Solar de Almería. Application to solar tower plants. Renew Energy 2019;136:1002–11. https://doi.org/10.1016/j.renene.2019.01.064.
[18] Ballestrín J, Monterreal R, Carra ME, Fernández-Reche J, Polo J, Enrique R, Rodríguez J, Casanova M, Barbero FJ, Alonso-Montesinos J, López G, Bosch JL, Batlles FJ, Marzo A. Solar extinction measurement system based on digital cameras. Application to solar tower plants. Renew Energy 2018;125:648–54. https://doi.org/10.1016/j.renene.2018.03.004.
[19] Heras C, Salinas I, Sevilla M, Chueca R, Escorza S, Fernández–Peruchena C, Bernardos A, Sevillano P, Sánchez M. Atmospheric attenuation measurement system for commercial solar plants based on optical spectrum analysis. Sol Energy 2022;236:782–9. https://doi.org/10.1016/J.SOLENER.2022.03.057.
[20] Tahboub ZM, Al Obaidli AA, Luque F, Salbidegoitia I, Farges O, Hassar Z, Oumbe A, Geuder N, Goebel O. Solar Beam Attenuation Experiments – Abu Dhabi, SolarPACES Conf 2012.
[21] Hanrieder N, Ghennioui A, Merrouni AA, Wilbert S, Wiesinger F, Sengupta M, Zarzalejo L, Schade A. Atmospheric transmittance model validation for CSP tower plants. Rem Sens 2019;11:1–18. https://doi.org/10.3390/rs11091083.
[22] Carra E, Ballestrín J, Monterreal R, Enrique R, Polo J, Fernández-Reche J, Barbero J, Marzo A, Alonso-Montesinos J, López G, Díaz B. Interannual variation of measured atmospheric solar radiation extinction levels. Sustain Energy Technol Assessments 2022;51:101991. https://doi.org/10.1016/J.SETA.2022.101991.
[23] Oka K, Mizutani W, Ashina S. Climate change impacts on potential solar energy production: a study case in Fukushima, Japan. Renew Energy 2020;153:249–60. https://doi.org/10.1016/J.RENENE.2020.01.126.
[24] de la Vara A, Gutiérrez C, González-Alemán JJ, Gaertner MÁ. Intercomparison study of the impact of climate change on renewable energy indicators on the mediterranean islands. Atmosphere 2020;11. https://doi.org/10.3390/atmos11101036.
[25] Cronin J, Anandarajah G, Dessens O. Climate change impacts on the energy system: a review of trends and gaps. Clim Change 2018;151:79–93. https://doi.org/10.1007/s10584-018-2265-4.
[26] Poddar S, Evans JP, Kay M, Prasad A, Bremner S. Estimation of future changes in photovoltaic potential in Australia due to climate change. Environ Res Lett 2021;16. https://doi.org/10.1088/1748-9326/ac2a64.
[27] Poddar S, Kay M, Prasad A, Evans JP, Bremner S. Changes in solar resource intermittency and reliability under Australia’s future warmer climate. Sol Energy 2023;266:112039. https://doi.org/10.1016/J.SOLENER.2023.112039.
[28] Santos AJL, Lucena AFP. Climate change impact on the technical-economic potential for solar photovoltaic energy in the residential sector: a case study for Brazil. Energy Clim. Chang. 2021;2:100062. https://doi.org/10.1016/J.EGYCC.2021.100062.
[29] Salvador P, Pey J, Pérez N, Querol X, Artíñano B. Increasing atmospheric dust transport towards the western Mediterranean over 1948–2020. Npj Clim. Atmos. Sci. 2022;5:1–10. https://doi.org/10.1038/s41612-022-00256-4.
[30] Eyring V, Bony S, Meehl GA, Senior CA, Stevens B, Stouffer RJ, Taylor KE. Overview of the coupled model Intercomparison project phase 6 (CMIP6) experimental design and organization. Geosci Model Dev (GMD) 2016;9:1937–58. https://doi.org/10.5194/gmd-9-1937-2016.
[31] I.P. on C.C. (IPCC). Climate change 2021 – the physical science basis: working group I contribution to the sixth assessment report of the intergovernmental panel on climate change. Cambridge: Cambridge University Press; 2023. https://doi.org/10.1017/9781009157896.
[32] Wyser K, van Noije T, Yang S, von Hardenberg J, O’Donnell D, Döscher R. On the increased climate sensitivity in the EC-Earth model from CMIP5 to CMIP6. Geosci Model Dev (GMD) 2020;13:3465–74. https://doi.org/10.5194/gmd-13-3465-2020.
[33] Wu T, Lu Y, Fang Y, Xin X, Li L, Li W, Jie W, Zhang J, Liu Y, Zhang L, Zhang F, Zhang Y, Wu F, Li J, Chu M, Wang Z, Shi X, Liu X, Wei M, Huang A, Zhang Y, Liu X. The Beijing Climate center climate system model (BCC-csm): the main progress

from CMIP5 to CMIP6. Geosci Model Dev (GMD) 2019;12:1573–600. https://doi.org/10.5194/gmd-12-1573-2019.
[34] O'Neill BC, Tebaldi C, Van Vuuren DP, Eyring V, Friedlingstein P, Hurtt G, Knutti R, Kriegler E, Lamarque JF, Lowe J, Meehl GA, Moss R, Riahi K, Sanderson BM. The scenario model Intercomparison project (ScenarioMIP) for CMIP6. Geosci Model Dev (GMD) 2016;9:3461–82. https://doi.org/10.5194/gmd-9-3461-2016.
[35] Hanrieder N, Wilbert S, Mancera-Guevara D, Buck R, Giuliano S, Pitz-Paal R. Atmospheric extinction in solar tower plants - a review. Sol Energy 2017;152:193–207. https://doi.org/10.1016/j.solener.2017.01.013.
[36] B.L. Kistler, A user's manual for DELSOL3: a computer code for calculating the optical performance and optimal system design for solar thermal central receiver plants, Other inf. Portions this doc. Are illegible microfich. Prod. Orig. Copy available until stock is exhausted. Incl. 5 sheets 48x reduct. Microfich. (1986) medium: X; size: Pages: 231. https://doi.org/SAND86-8018.
[37] Leary PL, Hankins JD. User's guide for MIRVAL – a computer coe for modeling the optical behavior of reflecting solar concentrators. Alburquerque, USA: Sandia Report; 1979. SAND77-8280.
[38] Wagner MJ, Wendelin T. SolarPILOT: a power tower solar field layout and characterization tool. Sol Energy 2018;171:185–96. https://doi.org/10.1016/j.solener.2018.06.063.
[39] Wendelin T. SolTRACE: a new optical modeling tool for concentrating solar optics. In: Isec 2003 int. Sol. Energy conf., New York: American society of mechanical engineers. Hawai: Kohala Coast; 2003. p. 253–60. NREL Report No. CP-550-32866., 15-18 March 2003.
[40] Blair N, Diorio N, Freeman J, Gilman P, Janzou S, Neises T, Wagner M, Blair N, Diorio N, Freeman J, Gilman P, Janzou S, Neises T, Wagner M. System advisor model (SAM) general description. Golden: CO; 2018. https://doi.org/10.1111/j.1532-5415.2009.02342.x., Version 2017.9.5.
[41] Tebaldi C, Arblaster JM, Knutti R. Mapping model agreement on future climate projections. Geophys Res Lett 2011;38:1–5. https://doi.org/10.1029/2011GL049863.
[42] Ballestrín J, Carra ME, Enrique R, Monterreal R, Fernández-Reche J, Polo J, Casanova M, Barbero FJ, Marzo A. Diagnosis of a Lambertian target in solar context. Measurement 2018;119:265–9. https://doi.org/10.1016/J.MEASUREMENT.2018.01.046.
[43] Simal N, Ballestrín J, Carra E, Marzo A, Polo J, Barbero J, Alonso-Montesinos J, López G. Typical solar extinction year at Plataforma Solar de Almería (Spain). Application to thermoelectric solar tower plants. Energy 2024;296:131242. https://doi.org/10.1016/J.ENERGY.2024.131242.
[44] Isaza A, Kay M, Evans JP, Prasad A, Bremner S. Maximizing photovoltaic potential and minimizing costs in a future warmer climate: the role of atmospheric aerosols and greenhouse gas emissions. Renew Energy 2023;219:119561. https://doi.org/10.1016/J.RENENE.2023.119561.
[45] NREL, PySAM Version 4.2.0, Accessed Febr. 2, 2024. (n.d.). https://github.com/NREL/pysam.